Supporting Information

Electrochemical CO Reduction Builds Solvent Water into Oxygenate Products

Yanwei Lum[†,‡,⊥], Tao Cheng[§,∥,⊥], William A. Goddard III*[,§,∥] and Joel W. Ager*[,†,‡]

[†]Joint Center for Artificial Photosynthesis and Materials Sciences Division, Lawrence Berkeley National Laboratory, California 94720, United States.

[‡]Department of Materials Science and Engineering, University of California, Berkeley, California 94720, United States.

[§]Joint Center for Artificial Photosynthesis, California Institute of Technology, Pasadena, California 91125, United States.

[∥]Materials and Process Simulation Center (MC139-74), California Institute of Technology, Pasadena, California 91125, United States.

[⊥]These authors contributed equally to this work.

*Email: wag@wag.caltech.edu (W.A.G.); jwager@lbl.gov (J.W.A.)

Contents

Experimental

Materials

Potassium carbonate (99.995% metals basis), potassium hydroxide (99.99% metals basis), ^{13}C carbon monoxide (<5 atom % ^{18}O, 99 atom % ^{13}C), nitric acid (70%), hydrochloric acid (37%), potassium phosphate monobasic (99.99% metals basis) and potassium phosphate dibasic (99.95% metals basis) were purchased from Sigma-Aldrich. Glassy carbon plates were purchased from Alfa Aesar. Selemion AMV anionic exchange membranes were purchased from Asahi Glass Co., Ltd. Oxygen-18 enriched water (>97% ^{18}O) was purchased from Medical Isotopes Inc. Certified composition of the oxygen-18 enriched water was 97.70 at.% ^{18}O, 1.20 at.% ^{17}O and 1.10 at.% ^{16}O (Lot number: 880). Si wafers of various orientations were purchased from UniversityWafer, Inc. The copper sputtering target (99.999%) was purchased from Kurt J. Lesker Company. All chemicals were used without further purification. Nitrogen (99.999%), argon (99.999%) and hydrogen (99.999%) were purchased from Praxair. Carbon monoxide (99.999% research purity) was purchased from Matheson Tri-gas Inc. Hydrogen, argon, nitrogen and carbon dioxide gas purifiers purchased from Valco Instruments Co. Inc were used on the gas feeds to the electrochemical cell and gas chromatograph. 18.2 MΩ deionized (DI) water was produced by a Millipore system and used for electrolyte preparation.

Preparation of oriented Cu surfaces

Cu (100), (111) and (751) oriented surfaces were prepared according to similar procedures as described by Jaramillo and co-workers.[1] Si wafers with different orientations were used as growth substrates to facilitate epitaxial growth of Cu. Cu films grown on Si (100), (110) and (111) wafers yield Cu orientations of (100), (111) and (751) respectively. The native oxide on the Si wafers was first removed via a HF etch and subsequent growth of the films was carried out using sputtering with an AJA International ATC Orion 5 sputtering system. In all cases, the thicknesses of the Cu films were controlled to be 200 nm thick using a quartz crystal monitor. Samples were kept in a N_2 filled glove box when not in use to minimize oxidation in ambient air.

Materials characterization

X-ray diffraction (XRD) was performed with a Rigaku Smartlab x-ray diffractometer in the 2-theta mode. The orientations of the (100) and (111) Cu films were checked using X-ray diffraction (Figure S23).

The orientations were also confirmed according to similar procedures reported by Koper and co-workers[2] as well as Yeo and co-workers[3]. Briefly, this was accomplished with cyclic voltammetry in Ar sparged 0.1 M KOH solution (Figure S24) in the potential range of -1.3V to -0.45V vs Ag/AgCl at a rate of 120 mVs^{-1}. OH^- adsorption and desorption peaks are unique and depend on the Cu surface and thus may be used to identify and confirm its orientation. Cyclic

voltammetry was also carried out after CO reduction to confirm that loss of the surface orientation did not take place (Figure S24).

Electrochemical measurements

For all electrochemical measurements described in this work, a Biologic SP-300 potentiostat was used. CO reduction was carried out using a custom-made electrochemical cell made of PEEK and fitted with Teflon o-rings for chemical inertness and durability. In this cell, the working and counter electrodes are both constrained to be 1 cm^2 and sit parallel to each other in order to ensure a uniform potential distribution across the working electrode surface. In all electrochemical experiments, glassy carbon was used as the counter electrode (anode) instead of Pt due to concerns regarding Pt dissolution.[4] In order to ensure that the electrolyte remains saturated with CO throughout electrolysis, CO gas was continuously introduced into the electrochemical cell at a rate of 5 sccm (using a mass-flow controller). A custom-made glass frit fabricated by Adams & Chittenden Scientific Glass was used to disperse the gas into the electrolyte as well as provide adequate convection in the electrochemical cell. Before carrying out CO reduction experiments, CO gas was allowed to flow through the electrolyte in the cathode chamber for at least 15 minutes to ensure that the electrolyte is saturated with CO. In order to separate the electrolyte in the cathode and anode chambers, a Selemion AMV anion exchange membrane was employed. Before use, the membrane was carefully rinsed with DI water and completely dried with a stream of N_2. The electrolyte volume used in both the cathode and anode were 1.5 ml each. Before use in experiments, the electrochemical cell was sonicated in 20 wt.% nitric acid for 1 hour. All bulk electrolysis $C^{16}O$ reduction experiments were conducted for 70 minutes in $H_2{}^{18}O$ electrolyte. $H_2{}^{18}O$ electrolyte was used for both the catholyte and anolyte. A leak-free Ag/AgCl electrode from Innovative Instruments, Inc was employed as a reference electrode. The accuracy of this reference electrode was ensured periodically by comparison with a custom-made reversible hydrogen electrode. In order to convert potentials vs Ag/AgCl to the RHE scale, the following equation as used:

$$E\ (\text{vs.RHE}) = E\ (\text{vs.Ag/AgCl}) + 0.197\ \text{V} + 0.0591\ \text{pH} \quad \text{(S1)}$$

where the pH was 11.3 for 0.05 M K_2CO_3, 13 for 0.1 M KOH and 14 for 1.0 M KOH. After saturation of the electrolyte with CO, the solution resistance was determined using potentiostatic electrochemical impedance spectroscopy (PEIS), scanning through a frequency range of 1 MHz to 10 Hz. The solution resistance was then post-corrected for after the experiment.

Product analysis

All gas product analysis (hydrogen, methane, carbon monoxide, ethylene and ethane) described in this work were performed using a MG#3 Gas Chromatograph from SRI Instruments, equipped with a 12" long HaySep D column and argon as the carrier gas. The electrochemical cell was linked directly to the gas chromatograph to enable continuous online analysis of the gas products. Detection of the hydrogen was achieved using a TCD detector and detection of the hydrocarbons

was achieved using a FID equipped with a methanizer. The gas chromatograph was calibrated using calibration tanks containing varying amounts of hydrogen, carbon monoxide, methane, ethylene and ethane. CO reduction experiments were carried out for 70 minutes and analysis of the gas products was done at the 10, 25, 40, 55 and 70 min marks. The average of these values was taken to give the reported data.

Liquid products were quantified and their isotopic composition determined using gas chromatography-mass spectrometry (GCMS) with an Agilent 7890A GC with 5975C inert XL MSD (triple axis detector). The column used was an Agilent J&W PoraPLOT Q capillary column of length 25 m, internal diameter 0.25 mm and film thickness 8 µm (part number CP7549). Helium (99.999%) was used as the carrier gas with a flow rate of 1.0 ml/min in the column. A glass wool liner was used in the inlet, which was set to 250 °C. Prior to injection, samples were first acidified with concentrated hydrochloric acid to pH 2 in order to convert acetate into the acetic acid form, which is amenable to GCMS analysis. For each analysis, 0.5 µl of sample was injected and the injection mode was split with a 25:1 ratio. The selected ion monitoring (SIM) operating mode was used. Elution times and mass spectra of the target analytes (methanol, ethanol, allyl alcohol, 1-propanol and acetic acid) were determined by injecting known standards dissolved in water. Quantification was accomplished by injecting known concentrations of standards to build calibration curves. To analyze methanol, the GCMS oven temperature was set to 100°C and held for 6 minutes. To analyze all other products, the oven temperature was set to 140 °C for 10 minutes. A bake out at 200 °C for 5 minutes was utilized at the end of every run.

To ensure that the mass spectra of different products obtained with our GCMS are consistent with established databases[5], standards of natural isotopic abundances were also injected and all mass fragments with m/z in the range 20 to 70 were scanned (Figures S2-5 and S7). Additionally, to ensure that the detection sensitivities for both ^{16}O and ^{18}O are similar for all products, a series of control experiments were carried out (see control experiments section for more details).

In addition, formation of methanol on the Cu (111) surface was confirmed with NMR using a Bruker Avance III 500 MHz spectrometer. Dimethoxy sulfoxide (DMSO) was used as the internal standard and solvent suppression techniques were employed to reduce the size of the water peak (Figure S8).

Computational Methods

We simulated the water/Cu (100) interface using 48 explicit water molecules on a 4×4 Cu (100) surface slab (3 layers). The simulation box was 40 Å along the z-axis with a vacuum of 24 Å. The lateral dimensions of the slab were fixed using the 3.61 Å lattice constant. Two CO molecules and one H atom were placed on the 4 × 4 unit cell (on top site) corresponding to a surface coverage of 1/8 and 1/16 ML respectively. We find that including one extra Na solvated in the solution leads to a work function of 3.40 (±0.25) eV, which corresponds to -0.59 V (RHE) (3.40 – 4.40 + 0.0591×7 = -0.59 V). We have found that this model of QM with explicit

treatment of the water dynamics at operating temperature provides a representative description of the reaction kinetics.

Electronic structure calculations were performed within the DFT framework, as implemented in the Vienna ab initio simulation program (VASP),[6–9] a planewave pseudopotential package. The exchange and correlation energies were calculated using the Perdew, Burke, and Ernzerhof (PBE) functional within the generalized gradient approximation (GGA).[10]. We used a plane-wave cutoff energy of 400 eV and the First order Methfessel-Paxton scheme with a smearing width of 0.2 eV. Dipole corrections were applied along the z axis. The PBE-D3 method was employed to correct van der Waals interaction of water-water and water-Cu.[11] The Energy minimization criterion was that all forces on free atoms be < 0.02 eV/Å. The PBE-D3 method was employed to correct van der Waals interaction of water-water and water-Cu.[11] Spin polarization did not have an appreciable effect on the overall energies. The calculations were therefore carried out without spin polarization to reduce computational demands.

To equilibrate the waters interacting with the interface, we carried out 2 ns of reactive molecular dynamics (RMD) simulations using the ReaxFF reactive force field for Cu and H_2O.[12] Starting from this well-equilibrated interface; we carried out 10 ps of ab initio molecular dynamics (AIMD) simulation at 298 K. After that, we used metadynamics and thermodynamic integration to calculate free energy barriers for various reaction steps (the results were averaged over three independent calculations).

We used a 1.2 fs time step in the Molecular Dynamics (MD) simulations with the hydrogen mass set to 2 atomic mass unit. These MD simulations used only the gamma point of the Brillouin zone with no consideration of symmetry. The velocities were rescaled every 20 MD steps to readjust the target temperature to equilibrium. We employed a Nose-Hoover thermostat for the free energy calculations with a temperature damping parameter of 100 fs.

Enhanced sampling methods can increase the time scale of brute force simulations. We calculated the free energies using metadynamics and Constrained Molecular Dynamics (blue moon ensemble)[13]. Three parameters are controllable and relevant to the accuracy of a metadynamics simulation: the height of a Gaussian hill (h), the width of the Gaussian hill (ω) and frequency to update the bias potential (t_G).[14,15] In this work, these parameters are h = 0.08 eV, ω = 0.18 Å and t_G = 24 fs. For the constrained molecular dynamics, we employed an increment of 0.67×10^{-3} Å/fs to the collective variables. We found that simulation times of 2.4 to 9.6 ps were sufficient to complete the reaction, depending on the reaction pathways. From the reactive trajectories, we selected 11 windows for thermodynamic integration calculations. 2.4 ps simulations were carried out at each window to produce the potential of mean force (PMF). Energy profiles were obtained by integrating the PMF. In this work we calculate the Helmholtz free energies (F), which we assume are similar to the Gibbs free energies (G).

Our calculations consider the pH effect implicitly basing on the results from pure water simulation (pH = 7) and the pH correction to RHE scale (equation S1), since our QM calculations were carried out at pH = 7 (pure water). Such corrections only applied to electrochemical reactions with OH^- production. For example, the reaction of *CO-CO + H_2O + e^- → *CO-COH + OH^- (Figure 3 in MS) has a free energy barrier of 0.14 eV at pH 7 (ref 18 in MS), which increases to 0.24 eV at pH 11.3 after applying the pH correction.

We carried out a QMD simulation with one NaOH explicitly included. This simulation leads to a reaction barrier for *CH-CH(OH) formation of 0.87 eV, slightly higher than that obtained from pure water simulation (0.81 eV) Accordingly, we conclude that the presence of OH^- has little influence on the rate of ^{18}O ethanol formation.

Gas chromatography – mass spectrometry product analysis

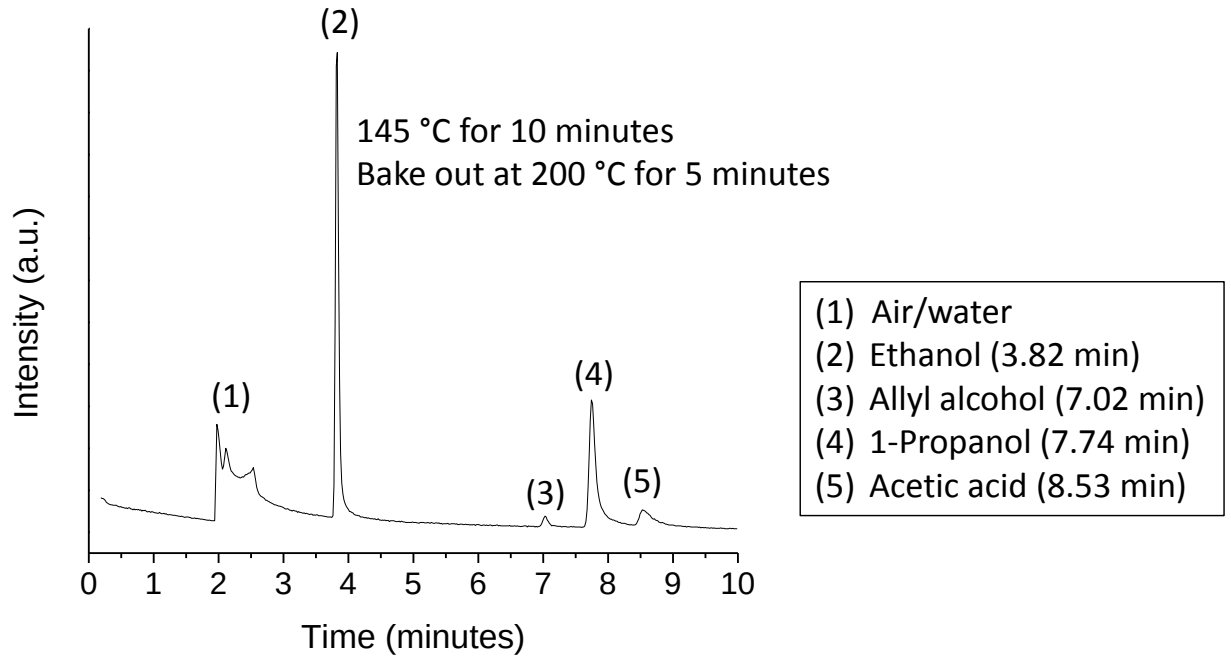

Figure S1. Typical chromatogram in GCMS analysis of a CO reduction sample. The operating mode is selected ion monitoring (SIM) to track ions of m/z: 31, 33. 46. 48, 57, 59, 60, 62 and 64. Operating at 145 °C for 10 minutes allows elution of ethanol, allyl alcohol, 1-propanol and acetic acid within 10 minutes. Products observed are ethanol, allyl alcohol, 1-propanol and acetic acid. Peaks are labeled according to the product and their elution times are listed as a legend in the figure.

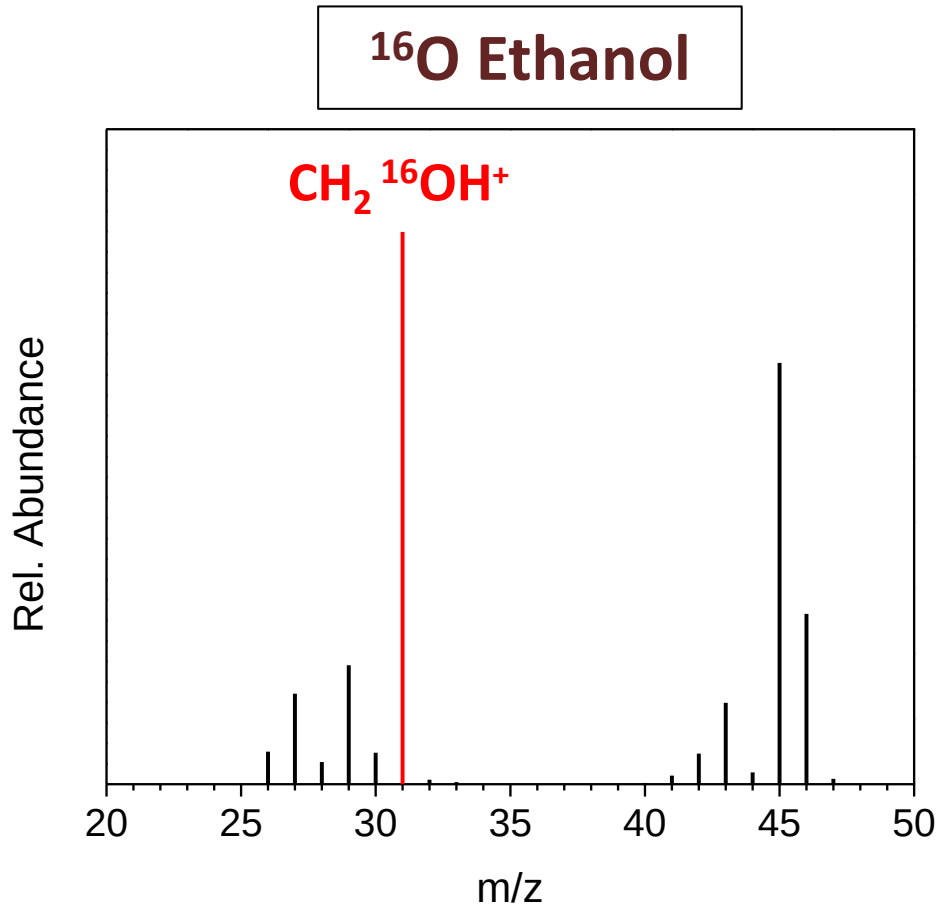

Figure S2. Typical mass spectrum of ^{16}O ethanol obtained on the GCMS instrument scanning all mass fragments with m/z in the range of 20 to 70. Data is in good agreement with the NIST database.[5] The fragment highlighted in red is the $CH_2{}^{16}OH^+$ fragment, which is utilized to determine the ^{18}O to ^{16}O ethanol ratio. To accurately determine the ^{18}O to ^{16}O ethanol ratio (isotopic composition), the choice of the mass fragment used for comparison is very important. For ^{16}O ethanol, we utilize mass fragment 31, which corresponds to the most abundant mass fragment, $CH_2{}^{16}OH^+$. For ^{18}O ethanol, we utilize mass fragment 33, which is not produced by ^{16}O ethanol and should correspond to $CH_2{}^{18}OH^+$. It is also important that ^{18}O ethanol does not produce a mass fragment of 31, which allows the ratio of m/z 33 to m/z 31 to exactly correspond to the ^{18}O to ^{16}O ethanol ratio. Fortunately, mass fragment 29 in ^{16}O ethanol is $C_2H_5{}^+$, which would not become mass fragment 31 in ^{18}O ethanol.

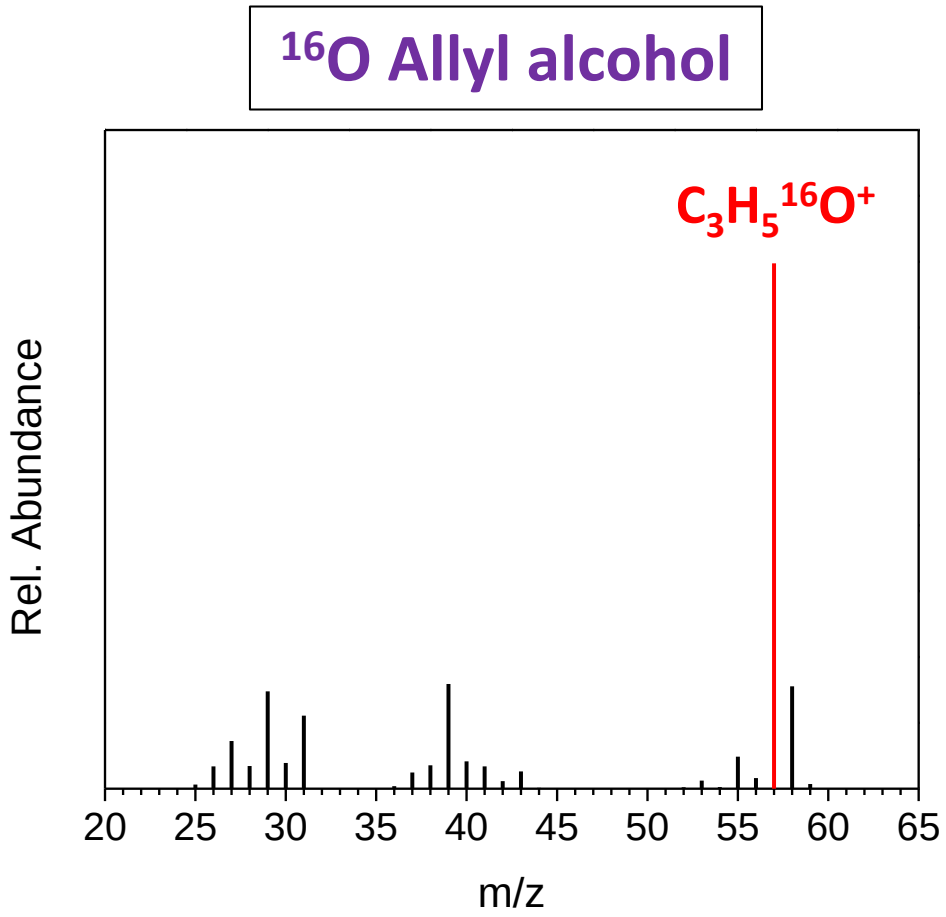

Figure S3. Typical mass spectrum of ^{16}O allyl alcohol obtained on the GCMS instrument by scanning all mass fragments with m/z in the range of 20 to 70. Data obtained is in good agreement with the NIST database.[5] The fragment highlighted in red is the $C_3H_5{}^{16}O^+$ fragment. For allyl alcohol, the isotopic composition can be determined by using the mass fragments 57 and 59 ($C_3H_5O^+$). Mass fragments 31 and 33 (CH_2OH^+) as well as 58 and 60 (C_3H_6O) can also be used. For all CO reduction conditions tested, ^{18}O allyl alcohol was not observed due to the absence of mass fragments 33, 59 and 60.

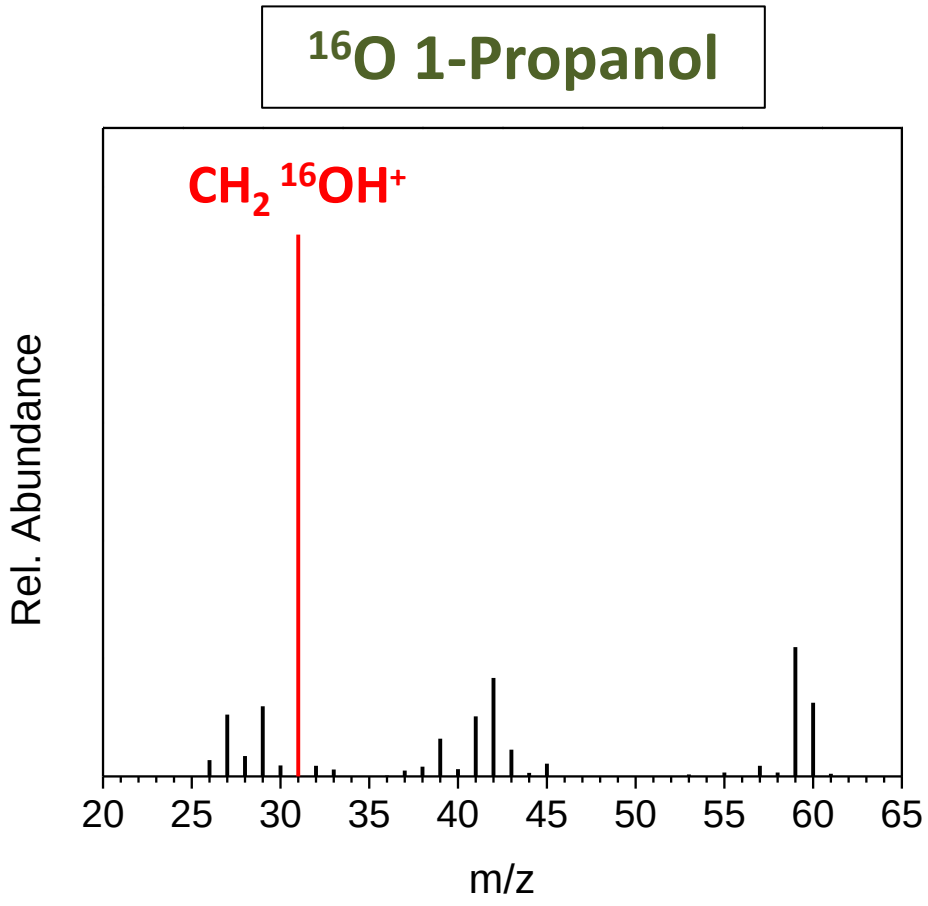

Figure S4. Typical mass spectrum of ^{16}O 1-propanol obtained on the GCMS instrument by scanning all mass fragments with m/z in the range of 20 to 70. Data obtained has good agreement with the NIST database.[5] The fragment highlighted in red is the $CH_2{}^{16}OH^+$ fragment, which is utilized to determine the ^{18}O to ^{16}O 1-propanol ratio. Determination of the isotopic composition of 1-propanol is very similar to that of ethanol. The ratio between mass fragments 31 and 33 (CH_2OH^+) are used, which corresponds to the fragment with the highest abundance.

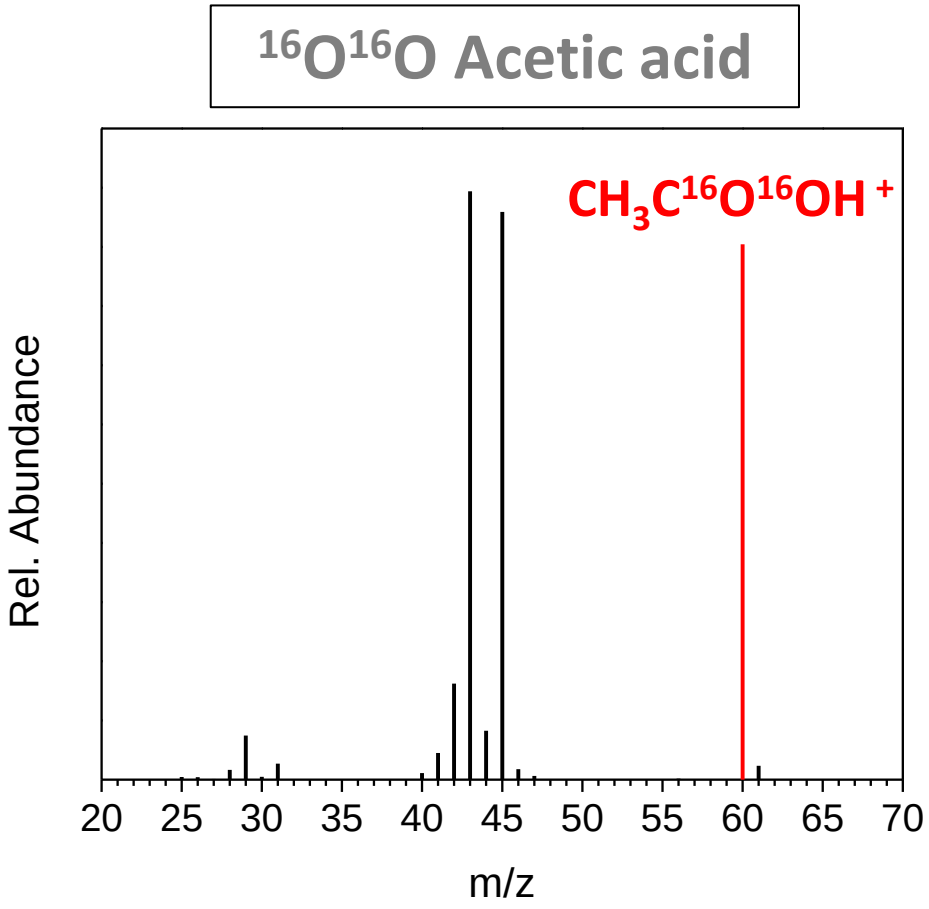

Figure S5. Typical mass spectrum of $^{16}O^{16}O$ acetic acid obtained on the GCMS instrument by scanning all mass fragments with m/z in the range of 20 to 70. Data obtained has good agreement with the NIST database.[5] The fragment highlighted in red is the $CH_3C^{16}O^{16}OH^+$ fragment, which is utilized to determine the $^{18}O^{18}O$, $^{16}O^{18}O$ and $^{16}O^{16}O$ acetic acid ratio. Determination of the isotopic composition of acetic acid is achieved by comparison of mass fragments 60 ($^{16}O^{16}O$), 62 ($^{16}O^{18}O$) and 64 ($^{18}O^{18}O$), which corresponds to the CH_3COOH^+ fragment. Usage of the other high abundance peaks of 43 and 45 is possible but not as accurate due to numerous overlapping fragments. For example, $^{16}O^{18}O$ acetic acid would produce m/z 45 and 47 fragments and $^{18}O^{18}O$ acetic acid would produce m/z 47 and 49 fragments.

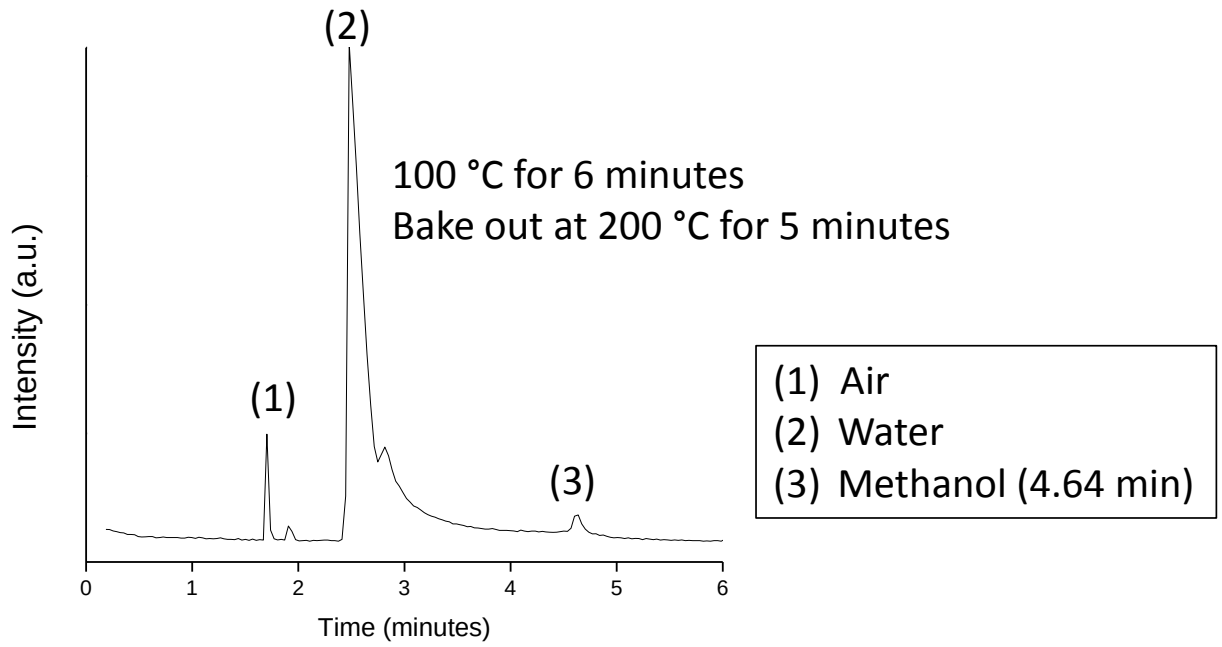

Figure S6. Typical chromatogram obtained for GCMS analysis of a CO reduction sample to detect methanol. Analysis of methanol requires a different GCMS analysis method, in which the oven is kept at a lower temperature. Selected ion monitoring mode was used to track ions of m/z: 15, 29, 30, 31, 33 and 34. Peaks are labeled according to the product and their elution times are listed as a legend in the figure.

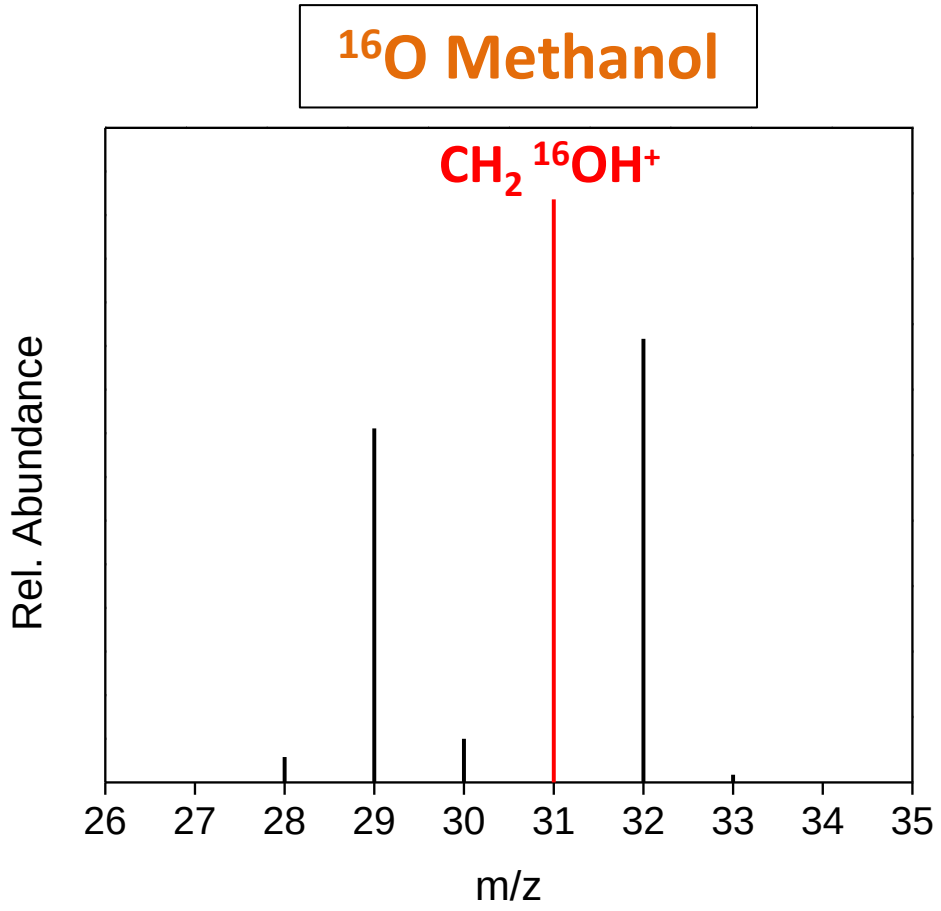

Figure S7. Typical mass spectrum of ^{16}O methanol obtained on the GCMS instrument by scanning all mass fragments with m/z in the range of 20 to 70. Data obtained has good agreement with the NIST database.[5] The fragment highlighted in red is the $CH_2{}^{16}OH^+$ fragment. For methanol, the presence of ^{18}O methanol can be verified by monitoring of the ions of m/z 33 and 34. These ions were not observed, which means that ^{18}O methanol was not produced. In addition, the formation of methanol on the Cu (111) surface at -0.65V vs RHE was confirmed by NMR (Figure S8).

NMR analysis

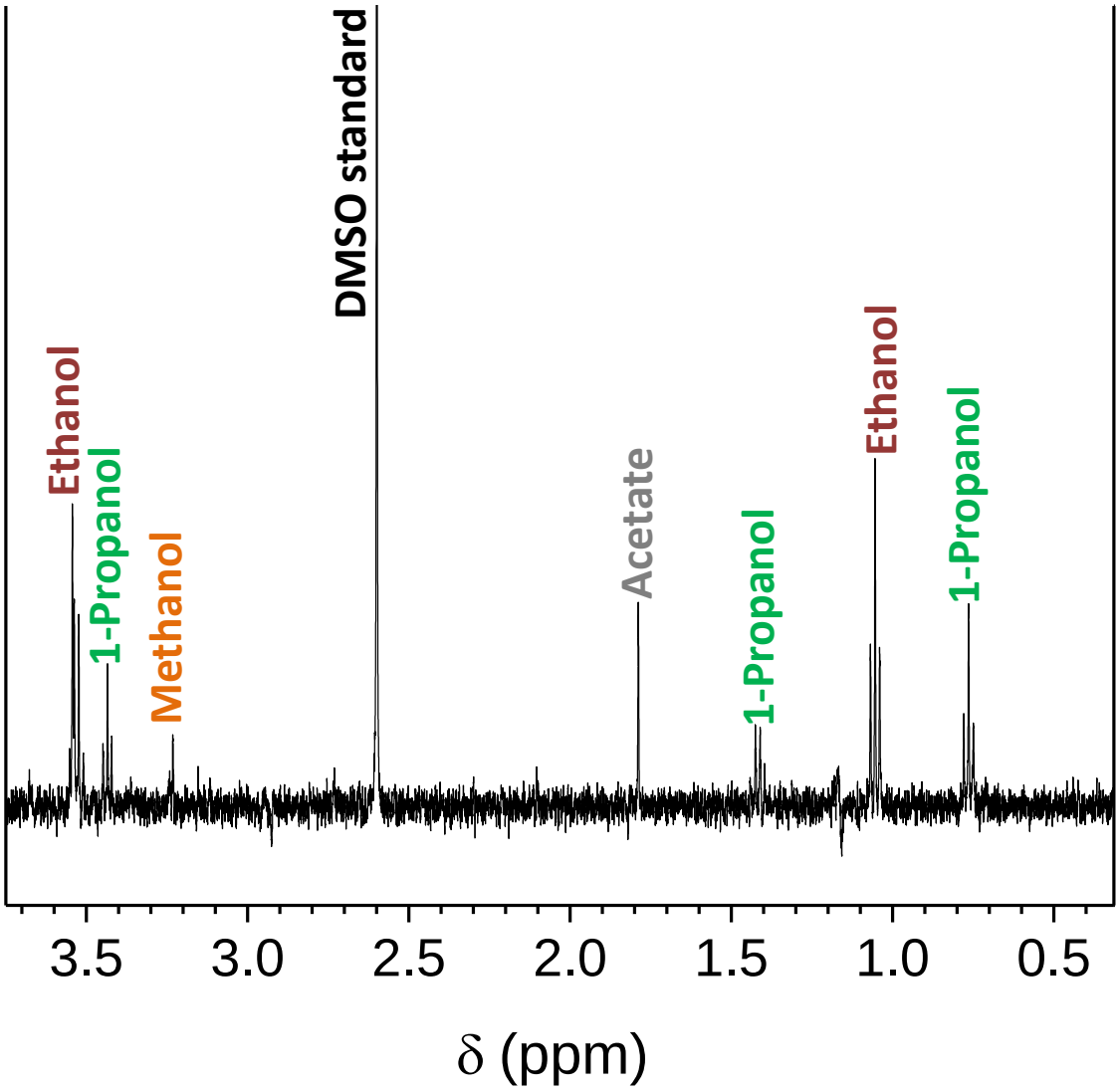

Figure S8. NMR spectra of the electrolyte from CO reduction with the Cu (111) surface at -0.65 V vs RHE. Methanol is labeled as a singlet peak located 3.23 ppm. Peaks corresponding to various other liquid products are labeled as well.

Control experiments

Control experiments were carried out to ensure that the ^{18}O incorporation into the various oxygenate products were not a result of homogenous reactions occurring in the bulk electrolyte.

Reaction between $C^{16}O$ and $H_2{}^{18}O$ to form $C^{18}O$

$C^{16}O$ could conceivably exchange to form $C^{18}O$ by interacting with ^{18}O water: $C^{18}O$ formed in this manner could then be reduced to ^{18}O ethanol. To rule this out, we bubbled $C^{16}O$ gas through ^{18}O water, and analyzed the gas exiting the cell with a GCMS. If exchange to form $C^{18}O$ had occurred, then a mass fragment of m/z 30 would be observed. Our experimental results (Figure S9) show that no mass fragment of m/z 30 was observed. Only mass fragments of m/z 28 and m/z 29 corresponding to $^{12}C^{16}O$ and $^{13}C^{16}O$ were observed, which rules out this form of isotope exchange.

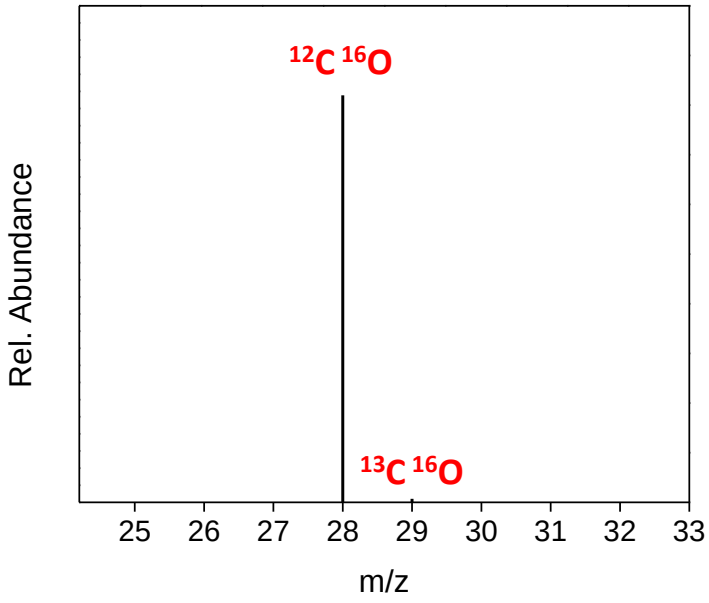

Figure S9. GCMS analysis of $C^{16}O$ that has been bubbled through ^{18}O water. Absence of mass fragment m/z 30 indicates that $C^{18}O$ is not formed, confirming that CO does not exchange O with water. The ^{13}C present (m/z 29) is due to the natural abundance of this isotope.

Reaction between products and $H_2{}^{18}O$

There could conceivably be a homogenous reaction by which ethanol, acetate and propanol exchange O with H_2O. This could, for example, convert an original ^{16}O ethanol to ^{18}O ethanol. To investigate this, we added 10 mM of ethanol, propanol and acetate into ^{18}O water containing 0.1 M KOH. After 1 hour, the solution was acidified to pH 2 and the isotopic composition was analyzed with GCMS. Figure S10 shows the relative intensities of the important mass fragments for each of the products. GCMS analysis was carried out approximately 20 minutes after

acidification, which was carried out in order to convert any acetate to acetic acid. As a comparison, the same experiment with ^{16}O water instead and the results are plotted in Figure S11.

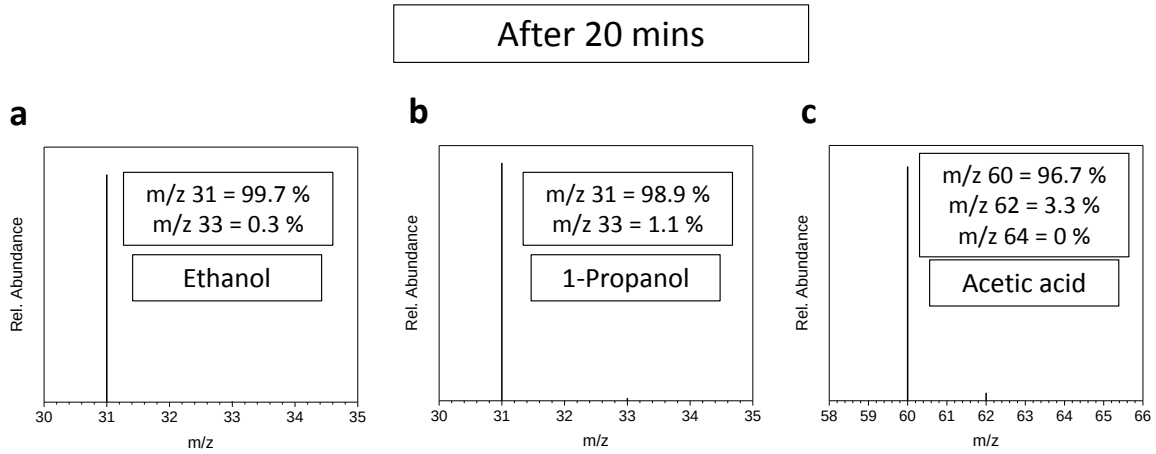

Figure S10. GCMS analysis of (a) ethanol, (b) propanol and (c) acetic acid that was added to ^{18}O water containing 0.1 M KOH. GCMS analysis was carried out approximately 20 minutes after acidification to pH 2.

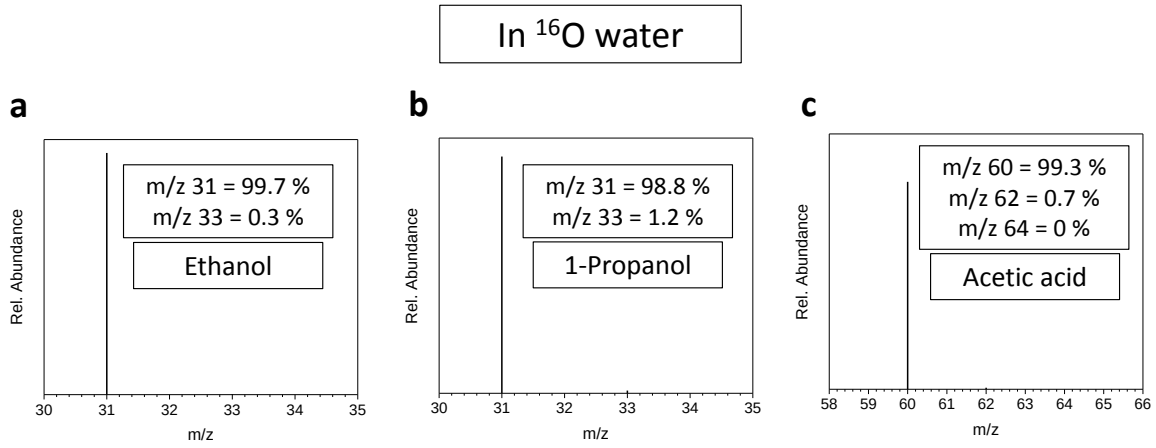

Figure S11. GCMS analysis of (a) ethanol, (b) propanol and (c) acetic acid that was added to ^{16}O water containing 0.1 M KOH. GCMS analysis was carried out after acidification to pH 2.

Based on the results in Figure S10 and S11, we see that major differences in the isotopic composition are not observed for ethanol and propanol (see Figures S2 and S4 for the rationale behind choosing m/z 31 and 33). For acetic acid, a small fraction of the $^{16}O^{16}O$ acetic acid (m/z 60) was observed to be transformed to $^{16}O^{18}O$ acetic acid (m/z 62). GCMS analysis of the same sample was carried out again after 3 hours and 18 hours and the results are shown in Figure S12 and S13 respectively.

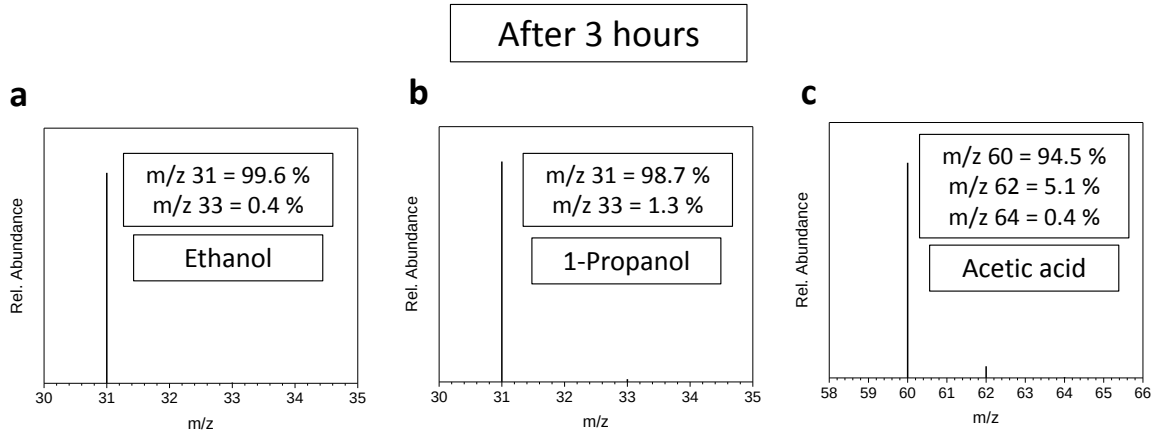

Figure S12. GCMS analysis of (a) ethanol, (b) propanol and (c) acetic acid that was added to ^{18}O water containing 0.1 M KOH. GCMS analysis was carried out approximately 3 hours after acidification to pH 2.

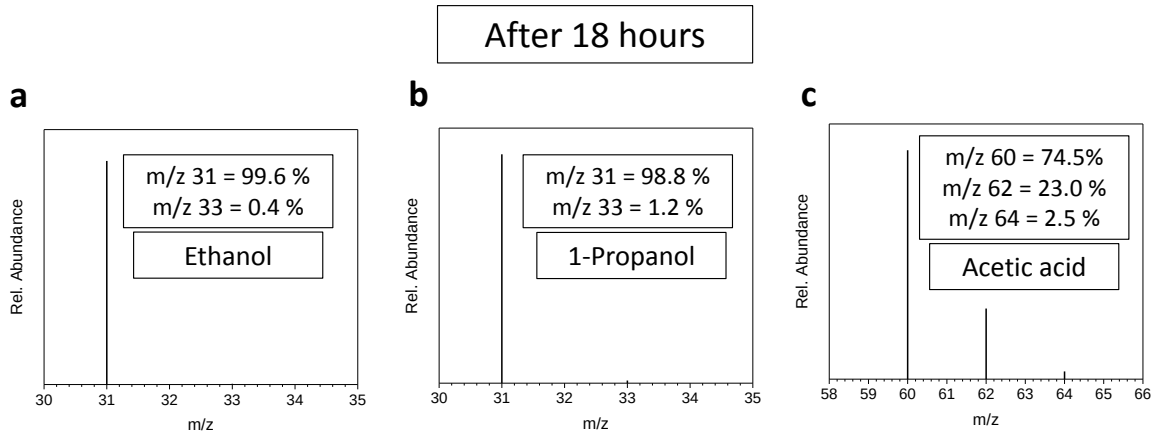

Figure S13. GCMS analysis of (a) ethanol, (b) propanol and (c) acetic acid that was added to ^{18}O water containing 0.1 M KOH. GCMS analysis was carried out approximately 18 hours after acidification to pH 2.

Figures S12 and S13 show that even after 3 and 18 hours in ^{18}O water, ethanol and propanol do not have significant changes in their isotopic compositions. On the other hand, there does appear to be a slow exchange of acetic acid with water. A small amount of $^{16}O^{16}O$ acetic acid was observed to convert to $^{16}O^{18}O$ acetic acid after 3 hours, and also $^{18}O^{18}O$ acetic acid began to appear (Figure S12c). After 18 hours (Figure S13c), a significant amount of the initial $^{16}O^{16}O$ acetic acid was observed to be converted into the $^{16}O^{18}O$ and $^{18}O^{18}O$ forms.

We therefore conclude that exchange of O between H_2O and ethanol and propanol does not occur under any of our experimental conditions. The acidification step used in the GCMS analysis does produce exchange between acetic acid and H_2O, but this happens at a slow rate. All

the GCMS analysis of the isotopic composition of acetic acid described in this work were done within 3 hours of acidification such that significant O exchange with the solvent does not occur.

Electrode mediated reaction between products and $H_2{}^{18}O$

It is conceivable that, in the presence of an electrode with an applied potential, an electrode mediated reaction might exist that would result in exchange of O between the products and $H_2{}^{18}O$. To explore this, we applied a current density of -5 mA cm^{-2} using a Cu working electrode with an electrolyte consisting of ^{18}O water with 0.1 M KOH and 10 mM of ethanol, propanol and acetate. After the electrolysis, the electrolyte was similarly acidified to pH 2 and the isotopic composition of the products was analyzed using GCMS after approximately 20 minutes (Figure S14). Based on the results, we rule out the possibility of any electrode mediated reaction causing exchange of O between the products and $H_2{}^{18}O$.

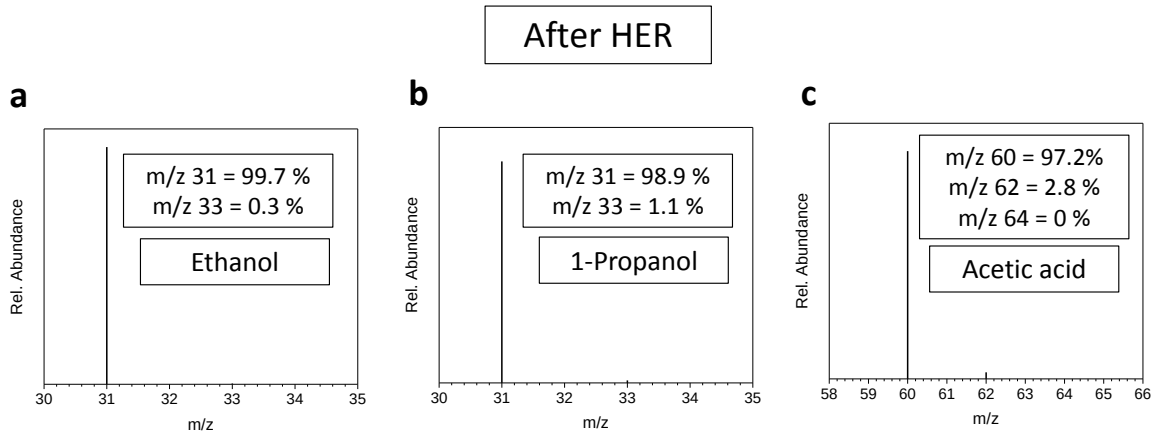

Figure S14. GCMS analysis of (a) ethanol, (b) propanol and (c) acetic acid that was added to ^{18}O water containing 0.1 M KOH. Electrolysis at -5 mA cm^{-2} with a Cu working electrode was carried out with this solution. GCMS analysis was carried out approximately 20 minutes after acidification to pH 2.

Cannizzaro-type disproportionation reactions

Koper and co-workers describe the possibility of Cannizzaro-type disproportionation reactions occurring during CO_2 reduction.[16] In such a process, the high local pH generated near the electrode surface causes this reaction to occur, converting an aldehyde (acetaldehyde) into the corresponding alcohol (ethanol) and carboxylate (acetate). Since the electrolytes we utilize are very alkaline, there is a possibility that this could account for the ^{18}O incorporation in our products. In the work described by Koper and co-workers[16], 50 mM of acetaldehyde was placed into alkaline solutions (pH 12-14), and small amounts (<0.4 mM) of acetate and ethanol were observed and attributed to a Cannizzaro-like process.

We performed a similar experiment but with a concentration of acetaldehyde which would be more typical of oxygenate concentrations attainable with our experimental conditions. When 1 mM of acetaldehyde was added to pH 14 water, we did not observe any ethanol or acetate

formation. This observation is consistent with similar experiments reported by Chorkendorff and co-workers.[17] This discrepancy can be rationalized by the fact that the Cannizzaro reaction is second order, requiring 2 aldehyde molecules and therefore would be expected to be highly dependent on the concentration of the reactant, which is very low in our case.

To further explore the possibility of Cannizzaro reactions, we carried out CO reduction with ^{18}O water containing 0.1 M K_2HPO_4 + 0.1 M KH_2PO_4 (phosphate buffer pH 7.2). Usage of the phosphate buffer was shown by Koper and co-workers to effectively suppress the Cannizzaro-like reaction.[16] Similarly, the isotopic composition of the products was analyzed with GCMS and are shown in Figure S15. Faradaic efficiency data are shown in Figure S16.

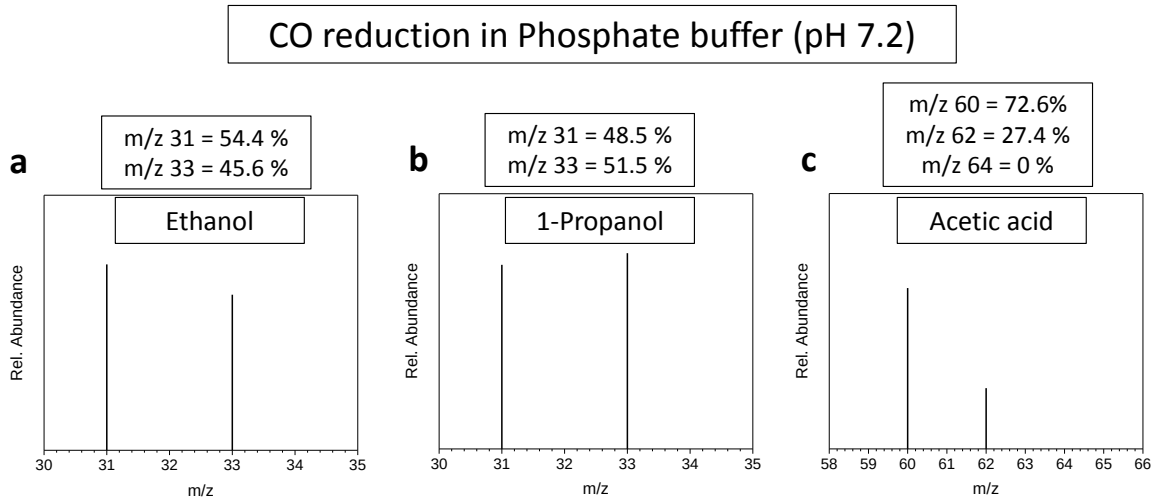

Figure S15. GCMS analysis of (a) ethanol, (b) propanol and (c) acetic acid. These products were generated by $C^{16}O$ reduction in ^{18}O water containing a phosphate buffer at pH 7.2.

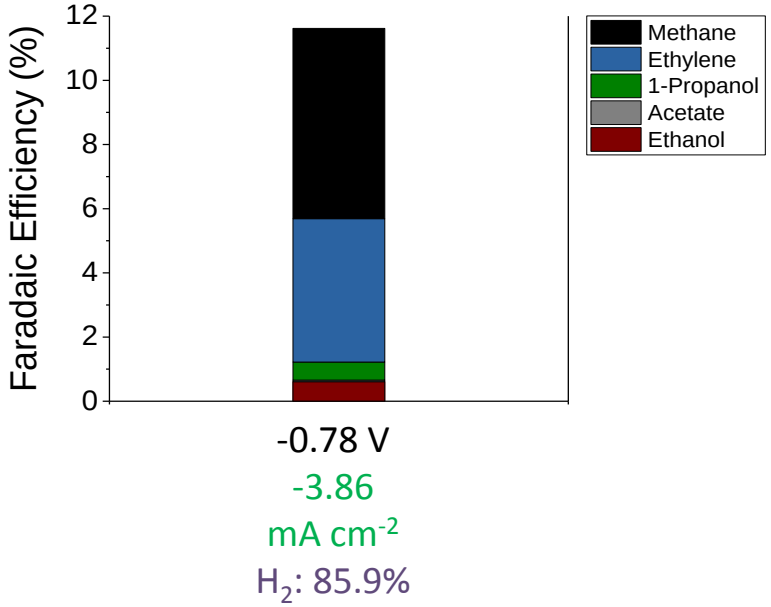

Figure S16. Faradaic efficiency data for CO reduction in ^{18}O water containing a phosphate buffer (pH 7.2). Observed total current density is shown in green font. Acetate was formed with a faradaic efficiency of only 0.05%. The balance FE is composed of hydrogen (shown in purple font). Potential shown is vs RHE.

Based on the isotopic composition, we observe that even with a phosphate buffer we see that a significant amount of ethanol (45.6 %) and propanol (51.5%) have ^{18}O. These results rule out Cannizzaro-type disproportionation reactions as the main route for incorporation of ^{18}O into the products.

Role of carbonate in ^{18}O product incorporation

In our experiments at pH 11.3, K_2CO_3 was used as the electrolyte and it is expected that CO_3^{2-} (carbonate) exchanges O rapidly with the solvent (^{18}O water).[18] If this ^{18}O-labeled carbonate could be electrochemically reduced, it would generate ^{18}O ethanol. However, this is not a concern because it is well known that carbonate or bicarbonate cannot be electrochemically reduced and CO_2 or CO is the reactant that reduces to products such as ethylene and ethanol.[19–22] Indeed, when a current density of -5 mA cm^{-2} was applied on a Cu foil electrode with Ar sparged 0.05 M K_2CO_3 (c.a. -1.8 V vs Ag/AgCl), only hydrogen was observed as a product. Therefore, ^{18}O carbonate or bicarbonate present in the electrolyte are not reduced to products such as ethanol under our experimental conditions. We also note that when $C^{16}O$ reduction was performed with ^{18}O water containing 0.1 M KOH and 1.0 M KOH, products were significantly enriched with ^{18}O (Figure 1). In these cases, neither carbonate nor bicarbonate were present in the electrolyte. Based on these observations, we conclude that exchange of O between the solvent and carbonate/bicarbonate cannot explain the ^{18}O enrichment we observe in our products.

To further rule out the role of carbonate in the formation of ethanol, we carried out $^{13}C^{16}O$ reduction in ^{16}O water with either $K_2{}^{12}CO_3$ or KOH as the electrolyte. If carbonate could be directly involved as reactant in the formation of ethanol, then we would observe that the relative intensities of the mass fragments of ethanol (especially the larger fragments) would depend on whether $K_2{}^{12}CO_3$ or KOH was used as the electrolyte, due to incorporation of ^{12}C from $K_2{}^{12}CO_3$.

To investigate this, a Cu (100) surface was used as the working electrode, using the same electrochemical cell with either 0.05 M $K_2{}^{12}CO_3$ or 0.1 M KOH as the electrolyte. In both cases, normal ^{16}O water was used as the solvent, a potential of -1.6 vs Ag/AgCl was applied for a duration of 40 minutes and ^{13}CO was flowed continuously during electrolysis at a flow rate of 5 sccm. Glassy carbon was used again as the counter electrode, with a Selemion AMV anion exchange membrane employed as well.

At the end of the electrolysis, the ethanol produced was analyzed with GCMS, using similar procedures as discussed in the methods section. In this case, mass fragments of m/z: 40, 41, 42, 43, 45, 46 and 48 were tracked in the selected ion monitoring (SIM) mode. Figure S17 and S18 shows the results for the case when $K_2{}^{12}CO_3$ or KOH was employed as the electrolyte

respectively. Table S1 compares the intensities of the various mass fragments normalized against the intensity of mass fragment m/z: 47. Based on the results, deviation of the relative intensities of the mass fragments between the two cases is not observed. This therefore further rules out the role of carbonate in ethanol formation.

Additionally, we performed the same reduction experiment on a 1:3 mix of ^{12}CO and ^{13}CO in 0.1 M KOH electrolyte in order to demonstrate the effect of ^{12}C incorporation of the relative intensities of the mass fragments of ethanol (Figure S19). Similarly, the relative intensities are normalized against mass fragment m/z: 47 (Table S2). As expected, the results are different from that when a pure ^{13}CO feed was used.

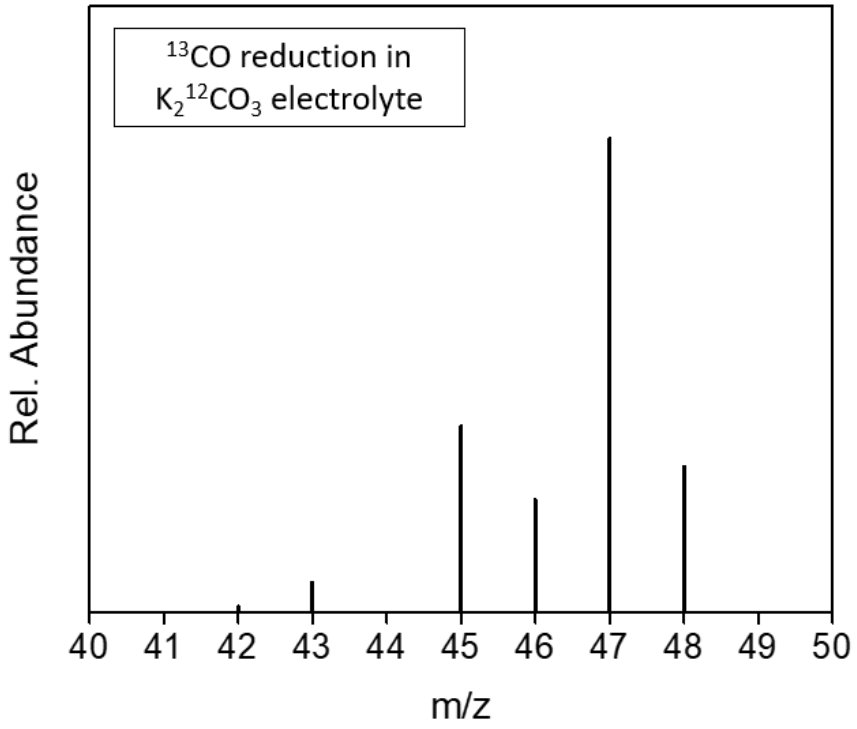

Figure S17 Relative abundances (intensities) of mass fragments of m/z: 42, 43, 45, 46, 47 and 48 of ethanol produced by the reduction of ^{13}CO in 0.05 M $K_2{}^{13}CO_3$ electrolyte.

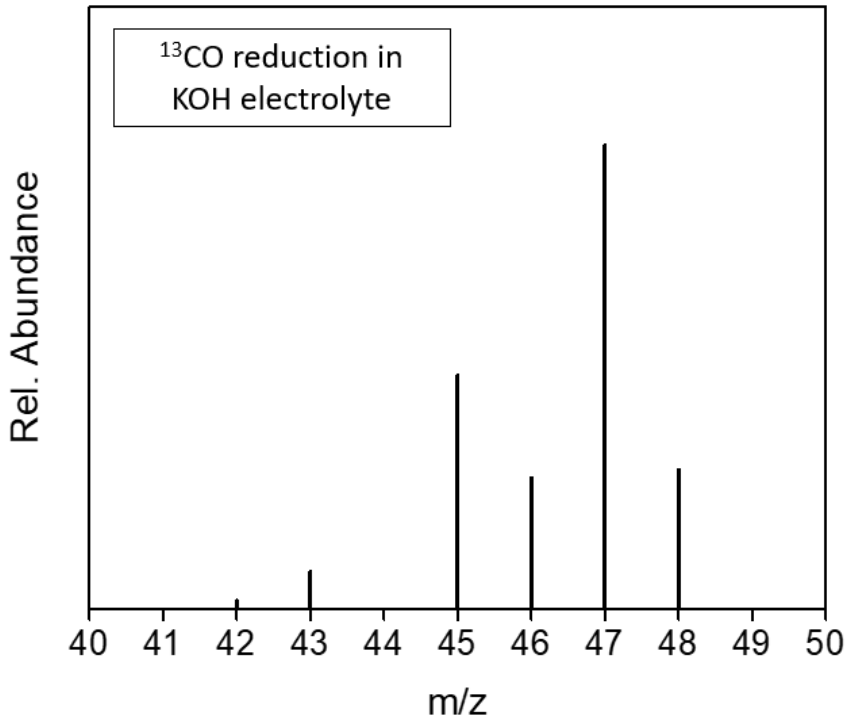

Figure S18 Relative abundances (intensities) of mass fragments of m/z: 42, 43, 45, 46, 47 and 48 of ethanol produced by the reduction of ^{13}CO in 0.1 M KOH electrolyte.

Table S1 Normalized intensities of various mass fragments of ethanol when ^{13}CO was reduced in either 0.05 M $K_2{}^{13}CO_3$ or 0.1 M KOH. The normalized intensities in both cases do not differ significantly from one another, ruling out carbonate as a reactant to produce ethanol.

Mass fragment	**Normalized intensity**	
	0.05 M $K_2{}^{13}CO_3$ electrolyte	0.1 M KOH electrolyte
42	0.011	0.017
43	0.062	0.079
45	0.391	0.502
46	0.236	0.282
47	1	1
48	0.306	0.299

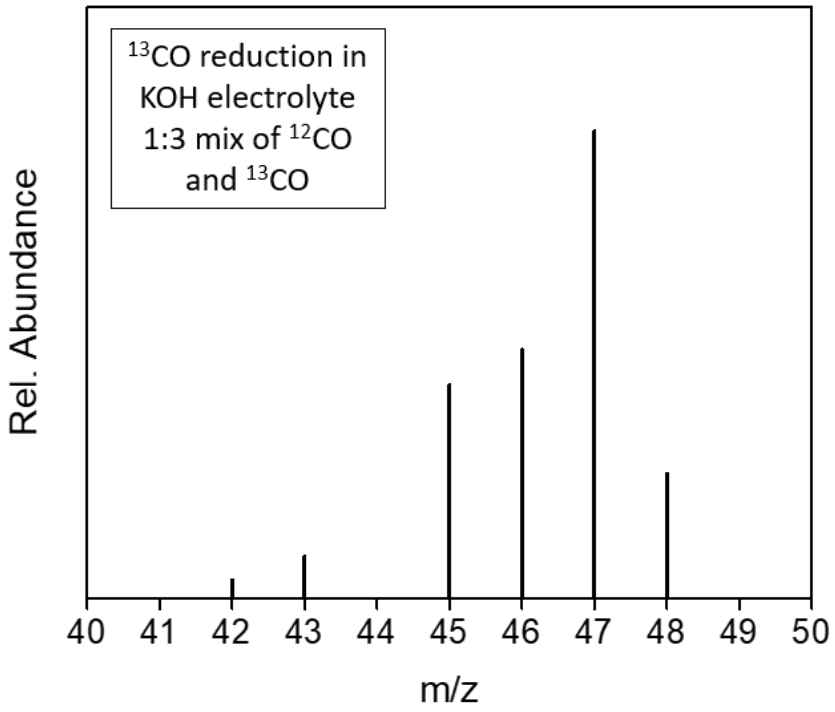

Figure S19 Relative abundances (intensities) of mass fragments of m/z: 42, 43, 45, 46, 47 and 48 of ethanol produced by the reduction of a mixed feed consisting of ^{12}CO ^{13}CO in a 1:3 ratio. The electrolyte used was 0.1 M KOH electrolyte.

Table S2 Normalized intensities of various mass fragments of ethanol produced by the reduction of a mixed feed consisting of ^{12}CO ^{13}CO in a 1:3 ratio. The electrolyte used was 0.1 M KOH electrolyte. As expected, the normalized intensities in this case differs from when a pure ^{13}CO feed was used.

Mass fragment	**Normalized intensity**
42	0.038
43	0.089
45	0.456
46	0.532
47	1
48	0.266

Relative MS sensitivity towards ^{16}O vs ^{18}O fragments

It is conceivable that the MS we employed might have different sensitivities towards ^{16}O vs ^{18}O fragments, which would affect the accuracy of the determination of the ^{18}O compositions of the various products. For example, if the MS were 3 times more sensitive to ^{16}O fragments and a 50:50 mixture of ^{18}O ethanol and ^{16}O ethanol were analyzed, we would determine the ^{18}O composition to be 25% instead of the true value of 50%. To rule out bias in the experimental results due to different isotope fragment detection sensitivities, we carried out a series of control experiments.

In a first approach, 2 separate samples each containing acetate, ethanol and 1-propanol were prepared. Sample A is enriched with ^{18}O, whereas the products in sample B are not (natural abundances). Their respective concentrations and ^{18}O compositions are as shown in Table S3. In this case, the concentrations were determined using HPLC using the procedure reported in our previous work.[23] Note that the isotopic compositions were determined by GCMS, assuming equal sensitivities for ^{18}O vs ^{16}O fragments.

Table S3 Concentrations and ^{18}O product compositions of ethanol, acetate and 1-propanol in a sample. Note that for acetate, the ^{18}O product composition corresponds to the percentage of $^{16}O^{18}O$ acetate, with the rest of the acetate being $^{16}O^{16}O$.

	Product	Concentration (mM)	^{18}O product composition (%)
Sample A	Ethanol	7.91	65.5
	Acetate	1.04	65.7
	1-propanol	0.976	89.8
Sample B	Ethanol	4.81	-
	Acetate	0.902	-
	1-propanol	0.835	-

To determine the relative sensitivity towards ^{16}O vs ^{18}O fragments, we mixed fixed amounts of sample A and B together and performed GCMS analysis on the products, as summarized in Table S4. Because we know the concentrations and ^{18}O composition of products in both sample A and B (Table S3), we can predict what the isotopic composition for any mixture should be. If the predictions fail to match with GCMS results, it would mean that the relative sensitivities of ^{16}O vs ^{18}O fragments are not similar.

Table S4 Amount of sample A and B mixed together as well as the predicted ^{18}O product compositions for each case. In all cases, 0.5 ml of sample A was used.

Amount of Sample A (ml)	Amount of Sample B (ml)	Predicted ^{18}O product composition (%)		
		Ethanol	Acetate	1-propanol
0.5	0.1	56.0	58.4	76.7
	0.2	48.8	52.7	66.9
	0.3	43.3	48.0	59.3
	0.4	38.8	44.1	53.3
	0.5	35.2	40.8	48.4
	0.6	32.3	37.9	44.3
	0.7	29.7	35.4	40.9

If the predicted ^{18}O composition and GCMS ^{18}O composition have similar values, we can say that the MS has similar sensitivities towards ^{16}O vs ^{18}O fragments. However, if the MS has significantly different sensitivities, we would see a disparity between the predicted and observed outcomes. Figure S20, S21 and S22 shows the predicted and GCMS ^{18}O compositions for ethanol, acetate and 1-propanol respectively. Excellent agreement is obtained between the predicted and measured values. As a result, we conclude that the MS has similar sensitivities to ^{18}O and ^{16}O mass fragments, which validates our experimental approach.

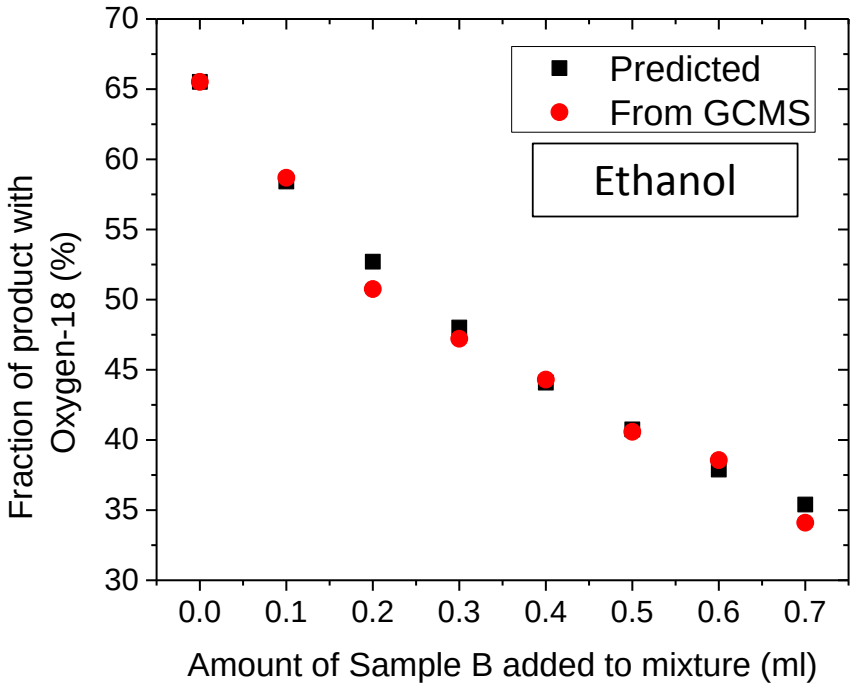

Figure S20 Predicted and GCMS ^{18}O compositions for ethanol. Good agreement is observed.

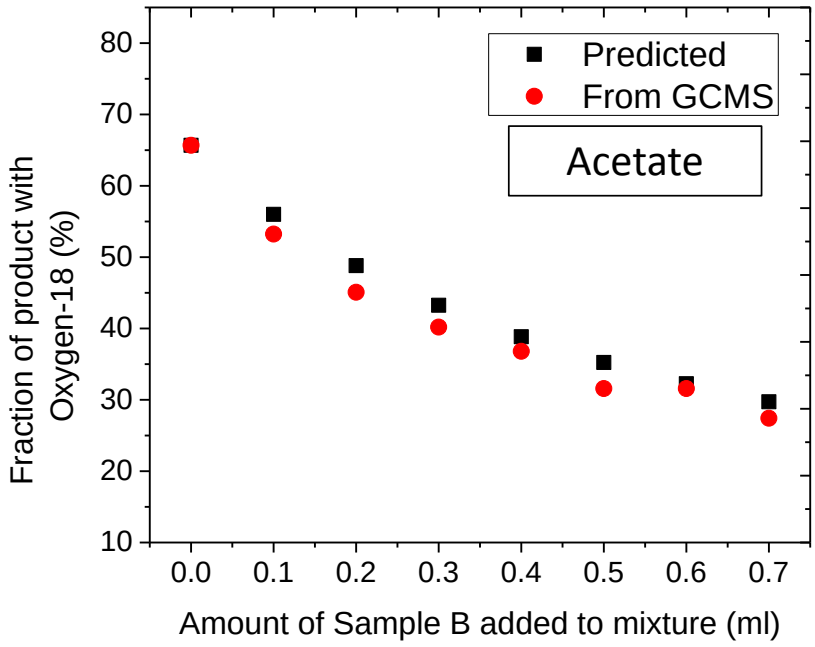

Figure S21 Predicted and GCMS ^{18}O compositions for acetate. Good agreement is observed.

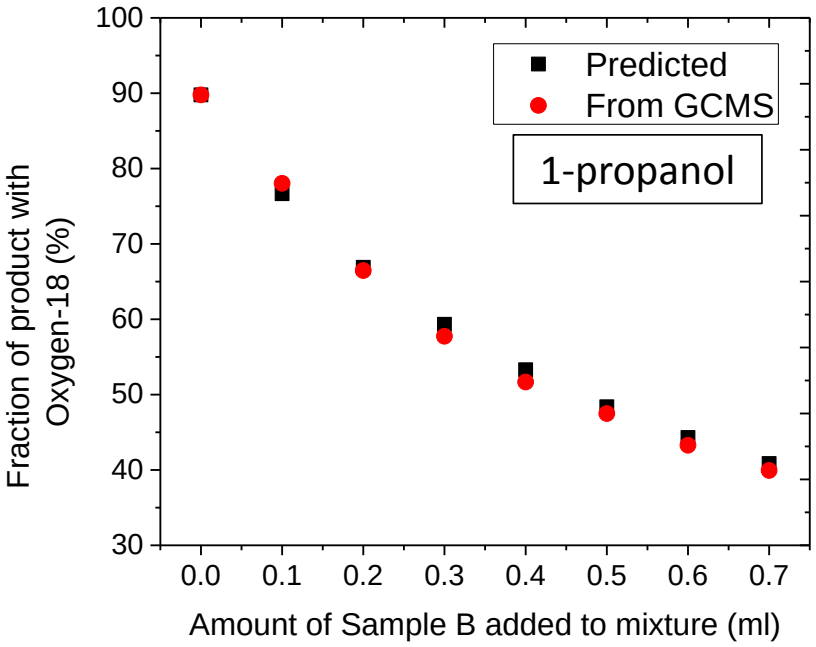

Figure S22 Predicted and GCMS ^{18}O compositions for 1-propanol. Good agreement is observed.

X-ray diffraction data

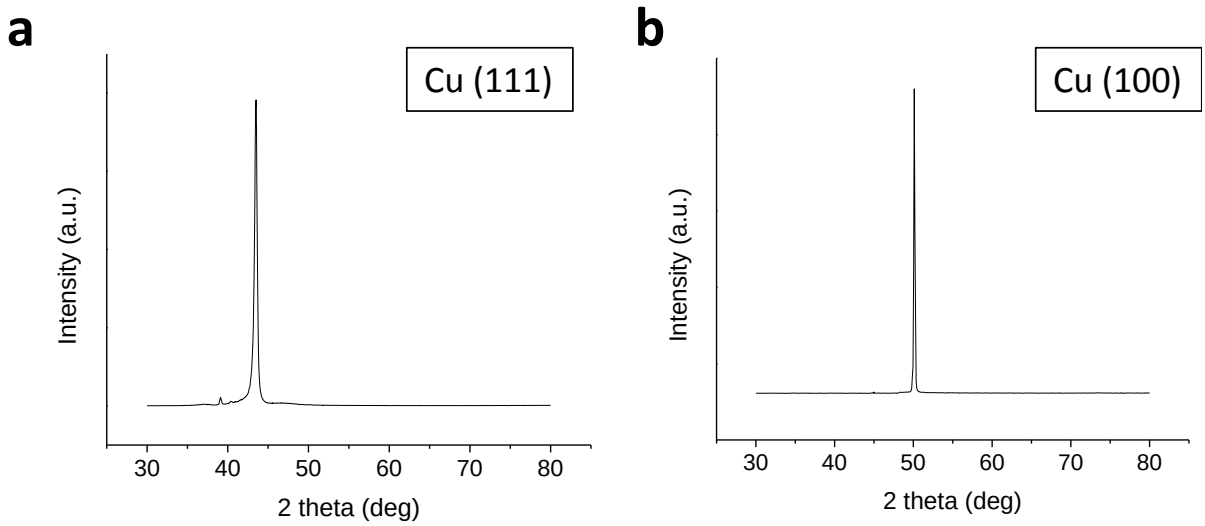

Figure S23. X-ray diffraction data for: (a) Cu (111) surface and (b) Cu (100) surface.

Electrochemical verification of surface orientation

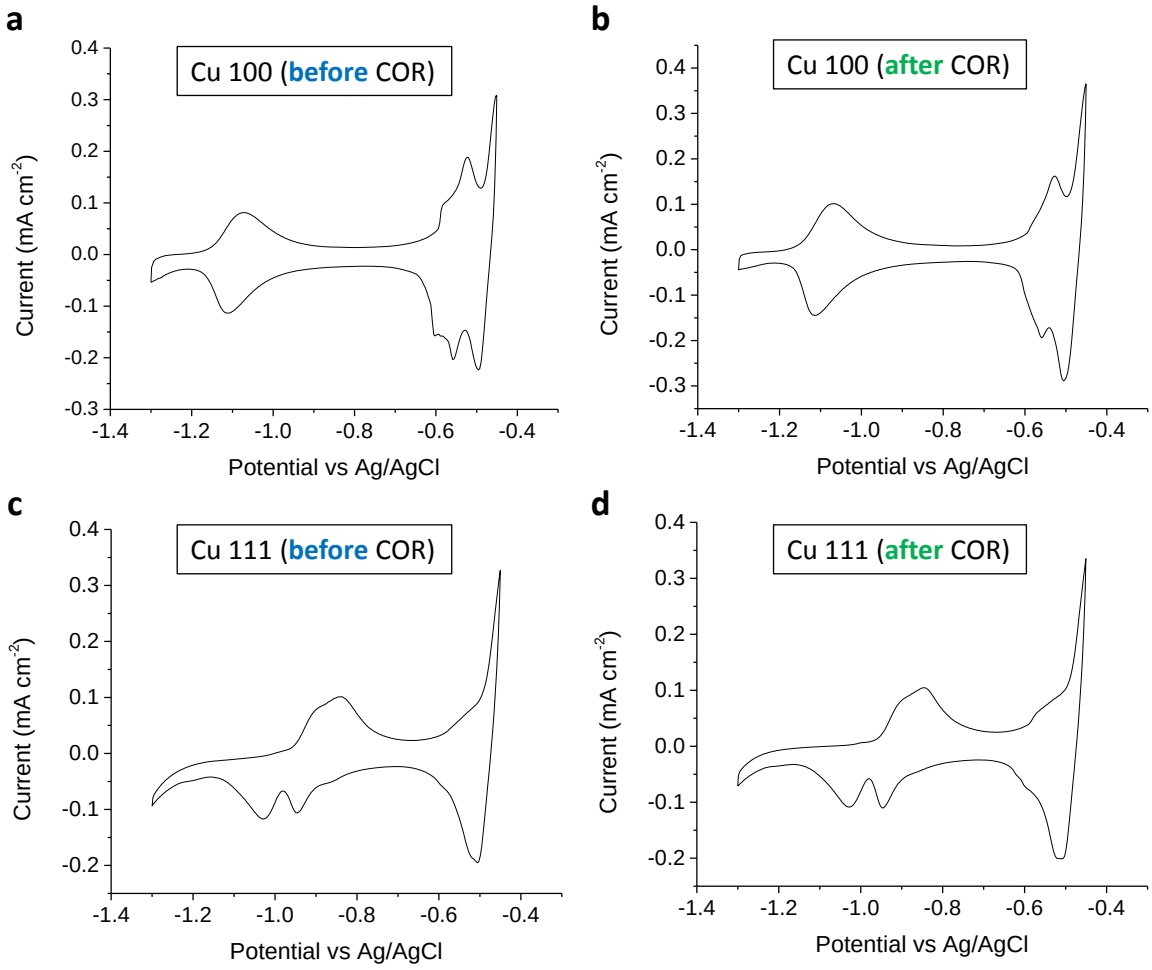

Figure S24. Cyclic voltammetry in Ar sparged 0.1M KOH electrolyte for Cu (100) before (a) and after (b) CO reduction respectively. Cyclic voltammetry in Ar sparged 0.1 M KOH electrolyte for Cu (111) before (c) and after (d) CO reduction respectively. This was done to confirm that the prepared Cu surfaces were oriented. This was also done after CO reduction to ensure that loss of surface orientation did not occur. The data obtained are consistent with the literature.[2,3] There are no major differences in the cyclic voltammogram before and after CO reduction, confirming that loss of surface orientation did not occur.

Faradaic efficiency data

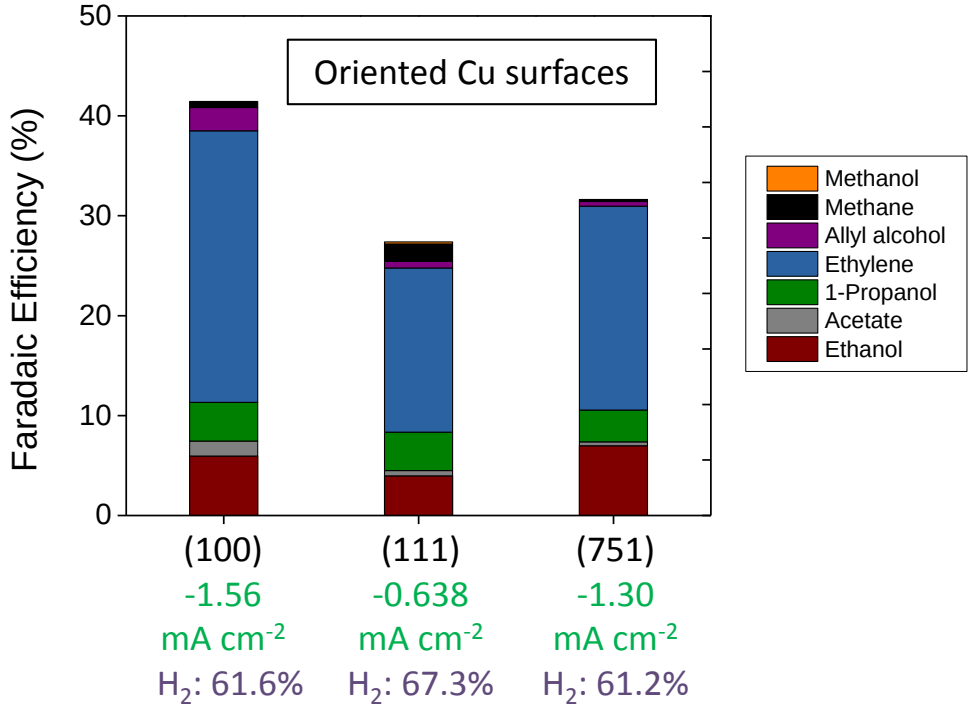

Figure S25. Faradaic efficiency for CO reduction on Cu (100), (111), and (751) orientations at c.a. -0.64V vs RHE. The balance is composed of hydrogen (shown in purple font). Experiments were done in 0.05 M K_2CO_3 (pH 11.3). Current densities are shown in green font.

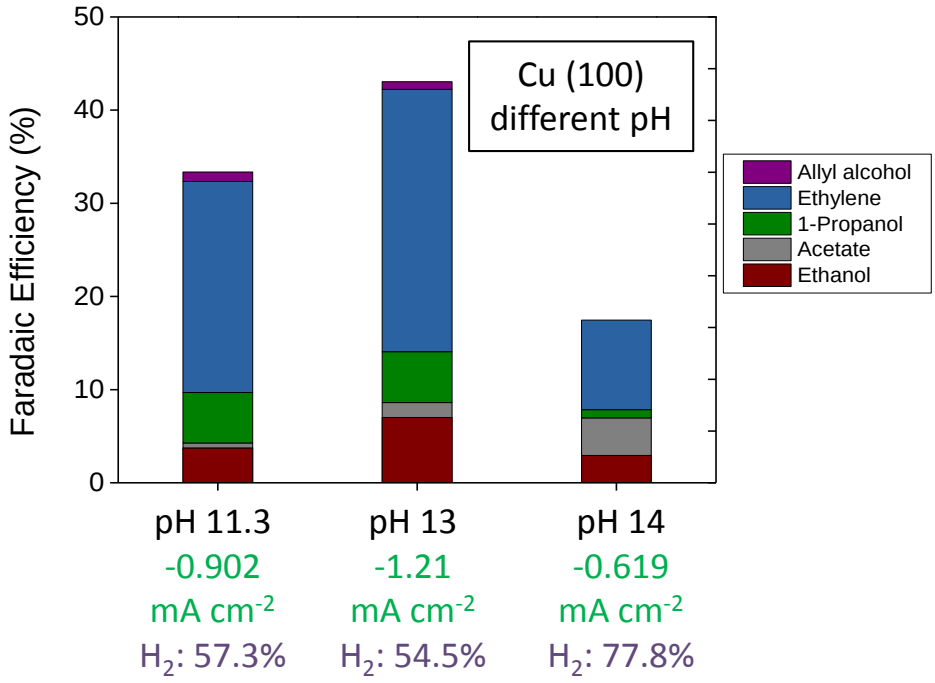

Figure S26. Faradaic efficiency for CO reduction on Cu (100) at pH 11.3, 13 and 14 at c.a. -0.53 V vs RHE. The balance is composed of hydrogen (shown in purple font). Current densities are shown in green font.

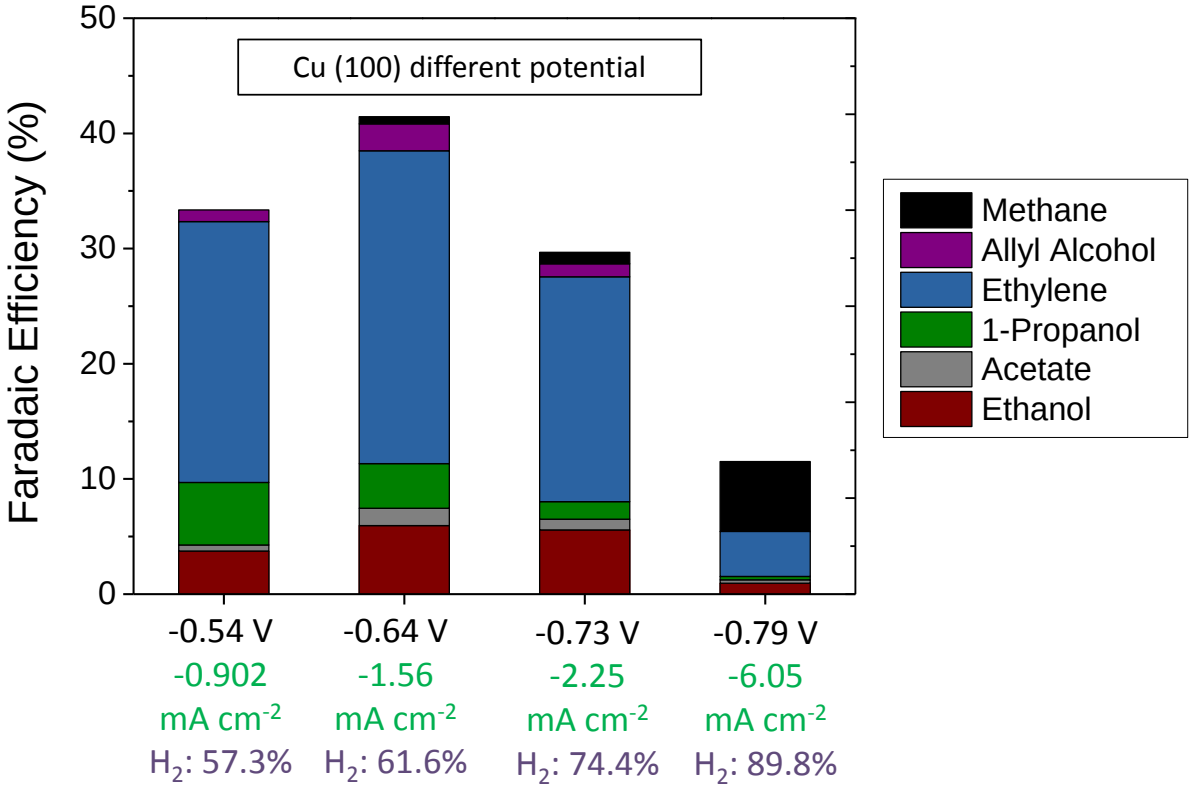

Figure S27. Faradaic efficiency for CO reduction on Cu (100) at various applied potentials. These experiments were conducted in 0.05 M K_2CO_3 (pH 11.3). The balance is composed of hydrogen (shown in purple font). Potentials are vs RHE scale and current densities are shown in green font.

Comparison of calculated energy barriers and experimental product formation ratios

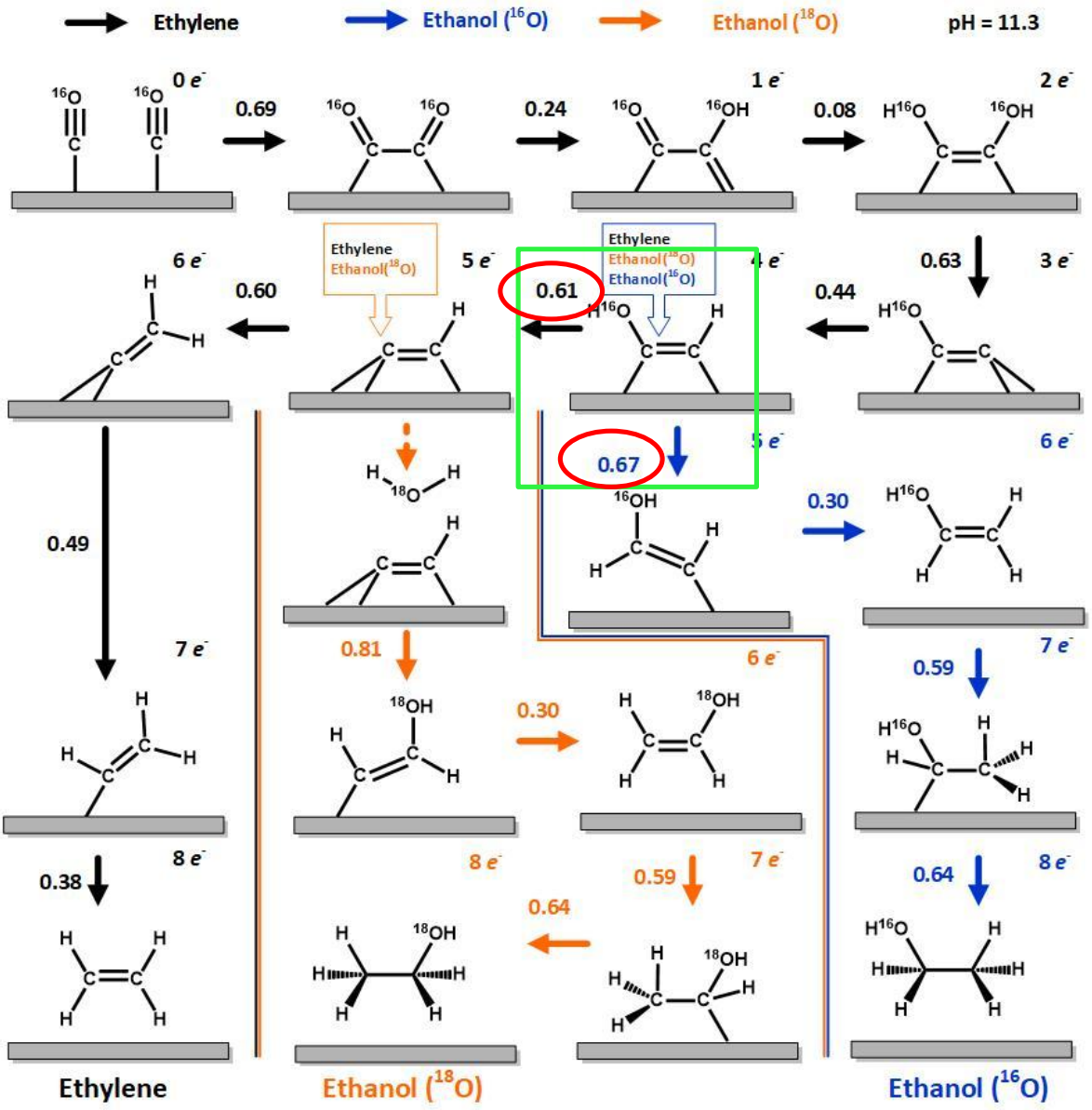

Figure S28. Modified version of Figure 3 in main text, in which the intermediate *(^{16}OH)C-CH is boxed in a green rectangle. *(^{16}OH)C-CH is a common intermediate for forming either ^{16}O ethanol or to ethylene + ^{18}O ethanol. The calculated barrier to form *C-CH is 0.61 eV (red circle) and this leads to ethylene and ^{18}O ethanol. The calculated barrier to form *H(^{16}OH)C-CH instead is 0.67 eV (red circle) and this intermediate leads to ^{16}O ethanol.

The Arrhenius equation can be used to calculate the predicted ratio of between these 2 branches and is carried out as follows:

Ratio = Exp[(Energy difference between barriers)*40] = Exp[(0.67-0.61)*40] = 11

The reverse calculation can be calculated from the experimental ratio to determine the energy difference between barriers. In the case of Cu (100) the experimental ratio (averaged between the 4 tested applied potentials) was 14. The calculation is as follows:

Energy difference between barriers = (1/40)*[ln(experimental ratio)]= (1/40)*[ln(14)]= 0.066 eV

Tautomers of acetaldehyde

It is well-known that the keto form (acetaldehyde, CH_3-CHO) is thermodynamically more stable than the enol form (ethenol, CH_2=CHOH). However, our QM metadynamics calculations (ref 18 in MS) finds that the reaction barrier for CH_2=CHOH to CH_3-CHO in solution to be 1.22 eV. On the other hand, the reaction barrier from CH_2=CHOH to surface adsorbed CH_3-*CHOH (a precursor of ethanol formation) is only 0.59 eV via the electrochemical reduction reaction. Thus, we estimate that the formation of CH_3-*CHOH is substantially faster than CH_2=CHOH. Thus, we consider that the absence of CH_3-CHO in our proposed reaction mechanism results from the slow reaction kinetics, despite the favorable thermodynamics.

Supplementary Movie 1

The reactive trajectory of concerted *CH-CH(OH) formation from *C-CH + H_2O. The 6 water molecules involved in the Grotthuss chain are shown in full. The other 48 water molecules not involved in the chain are faded out.

References

(1) Hahn, C.; Hatsukade, T.; Kim, Y.-G.; Vailionis, A.; Baricuatro, J. H.; Higgins, D. C.; Nitopi, S. A.; Soriaga, M. P.; Jaramillo, T. F. Engineering Cu Surfaces for the Electrocatalytic Conversion of CO_2 : Controlling Selectivity toward Oxygenates and Hydrocarbons. *Proc. Natl. Acad. Sci.* **2017**, *114* (23), 5918–5923.

(2) Pérez-Gallent, E.; Marcandalli, G.; Figueiredo, M. C.; Calle-Vallejo, F.; Koper, M. T. M. Structure- and Potential-Dependent Cation Effects on CO Reduction at Copper Single-Crystal Electrodes. *J. Am. Chem. Soc.* **2017**, *139* (45), 16412–16419.

(3) Huang, Y.; Handoko, A. D.; Hirunsit, P.; Yeo, B. S. Electrochemical Reduction of CO_2 Using Copper Single-Crystal Surfaces: Effects of CO* Coverage on the Selective Formation of Ethylene. *ACS Catal.* **2017**, *7* (3), 1749–1756.

(4) Chen, J. G.; Jones, C. W.; Linic, S.; Stamenkovic, V. R. Best Practices in Pursuit of Topics in Heterogeneous Electrocatalysis. *ACS Catal.* **2017**, *7* (9), 6392–6393.

(5) NIST Mass Spec Data Center, S.E. Stein, director, "Mass Spectra" in NIST Chemistry WebBook, NIST Standard Reference Database Number 69, Eds. P.J. Linstrom and W.G. Mallard, National Institute of Standards and Technology, Gaithersburg MD, 20899.

(6) Kresse, G.; Hafner, J. Ab Initio Molecular Dynamics for Liquid Metals. *Phys. Rev. B* **1993**, *47* (1), 558–561.

(7) Kresse, G.; Hafner, J. Ab Initio Molecular-Dynamics Simulation of the Liquid-Metal–amorphous-Semiconductor Transition in Germanium. *Phys. Rev. B* **1994**, *49* (20), 14251–14269.

(8) Kresse, G.; Furthmüller, J. Efficiency of Ab-Initio Total Energy Calculations for Metals and Semiconductors Using a Plane-Wave Basis Set. *Comput. Mater. Sci.* **1996**, *6* (1), 15–50.

(9) Kresse, G.; Furthmüller, J. Efficient Iterative Schemes for Ab Initio Total-Energy Calculations Using a Plane-Wave Basis Set. *Phys. Rev. B - Condens. Matter Mater. Phys.* **1996**, *54* (16), 11169–11186.

(10) Perdew, J.; Chevary, J.; Vosko, S.; Jackson, K.; Pederson, M.; Singh, D.; Fiolhais, C. Erratum: Atoms, Molecules, Solids, and Surfaces: Applications of the Generalized Gradient Approximation for Exchange and Correlation. *Phys. Rev. B* **1993**, *48* (7), 4978–4978.

(11) Grimme, S.; Antony, J.; Ehrlich, S.; Krieg, H. A Consistent and Accurate Ab Initio Parametrization of Density Functional Dispersion Correction (DFT-D) for the 94 Elements H-Pu. *J. Chem. Phys.* **2010**, *132* (15).

(12) Mueller, J. E.; Van Duin, A. C. T.; Goddard, W. A. Development and Validation of Reaxff Reactive Force Field for Hydrocarbon Chemistry Catalyzed by Nickel. *J. Phys. Chem. C* **2010**, *114* (11), 4939–4949.

(13) Sprik, M.; Ciccotti, G. Free Energy from Constrained Molecular Dynamics. *J. Chem. Phys.* **1998**, *109* (18), 7737–7744.

(14) Ensing, B.; Laio, A.; Parrinello, M.; Klein, M. L. A Recipe for the Computation of the Free Energy Barrier and the Lowest Free Energy Path of Concerted Reactions. *J. Phys. Chem. B* **2005**, *109* (14), 6676–6687.

(15) Laio, A.; Rodriguez-Fortea, A.; Gervasio, F. L.; Ceccarelli, M.; Parrinello, M. Assessing the Accuracy of Metadynamics. *J. Phys. Chem. B* **2005**, *109* (14), 6714–6721.

(16) Birdja, Y. Y.; Koper, M. T. M. The Importance of Cannizzaro-Type Reactions during

Electrocatalytic Reduction of Carbon Dioxide. *J. Am. Chem. Soc.* **2017**, *139* (5), 2030–2034.

(17) Bertheussen, E.; Verdaguer-Casadevall, A.; Ravasio, D.; Montoya, J. H.; Trimarco, D. B.; Roy, C.; Meier, S.; Wendland, J.; Nørskov, J. K.; Stephens, I. E. L.; et al. Acetaldehyde as an Intermediate in the Electroreduction of Carbon Monoxide to Ethanol on Oxide-Derived Copper. *Angew. Chemie Int. Ed.* **2016**, *55* (4), 1450–1454.

(18) Wang, X.; Conway, W.; Burns, R.; McCann, N.; Maeder, M. Comprehensive Study of the Hydration and Dehydration Reactions of Carbon Dioxide in Aqueous Solution. *J. Phys. Chem. A* **2010**, *114* (4), 1734–1740.

(19) Hori, Y. Electrochemical CO_2 Reduction on Metal Electrodes. In *Modern Aspects of Electrochemistry SE - 3*; Vayenas, C., White, R., Gamboa-Aldeco, M., Eds.; Modern Aspects of Electrochemistry; Springer New York: New York, NY, 2008; Vol. 42, pp 89–189.

(20) Zhong, H.; Fujii, K.; Nakano, Y. Electroactive Species Study in the Electrochemical Reduction of CO_2 in $KHCO_3$ Solution at Elevated Temperature. *J. Energy Chem.* **2016**, *25* (3), 517–522.

(21) Dunwell, M.; Lu, Q.; Heyes, J. M.; Rosen, J.; Chen, J. G.; Yan, Y.; Jiao, F.; Xu, B. The Central Role of Bicarbonate in the Electrochemical Reduction of Carbon Dioxide on Gold. *J. Am. Chem. Soc.* **2017**, *139* (10), 3774–3783.

(22) Zhu, S.; Jiang, B.; Cai, W.-B.; Shao, M. Direct Observation on Reaction Intermediates and the Role of Bicarbonate Anions in CO_2 Electrochemical Reduction Reaction on Cu Surfaces. *J. Am. Chem. Soc.* **2017**, *139* (44), 15664–15667.

(23) Lum, Y.; Yue, B.; Lobaccaro, P.; Bell, A. T.; Ager, J. W. Optimizing C-C Coupling on Oxide-Derived Copper Catalysts for Electrochemical CO_2 Reduction. *J. Phys. Chem. C* **2017**, *121* (26), 14191–14203.